Electronic Supporting Information (ESI) for:

How an organogelator can gelate water: Gelation transfer from oil to water induced by a nanoemulsion

Vivien Nouri, Marigilson Pontes De Siqueira Moura, Bruno Payre, Olivier De Almedia, Christophe Déjugnat, Sophie Franceschi, Emile Perez*

Table of Contents

1. Samples compositions and preparations

1.1. Chemical structures

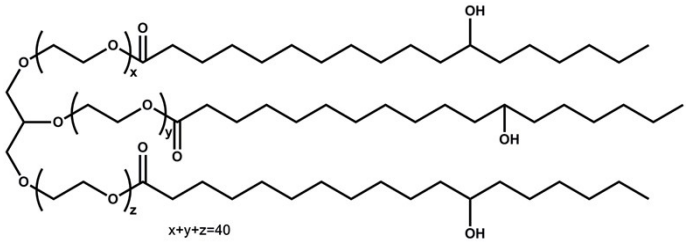

Kolliphor RH 40 (main component)

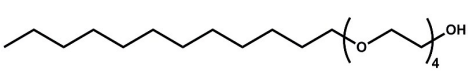

Brij L4

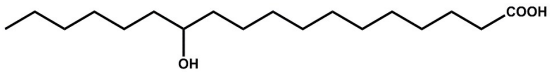

12-HOA

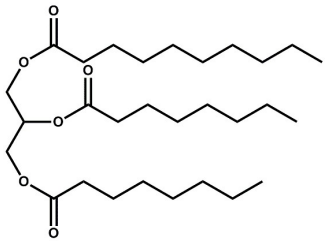

Miglyol 812 (main component)

Fig. S1 Chemical structures of the compounds entering into the composition of the gelled nanoemulsion

1.2. Preparation of the nanoemulsion

The nanoemulsion was prepared using the phase inversion temperature (PIT) method. Kolliphor® RH 40 (0.68 g) and Brij® L4 (0.32 g) surfactants were mixed with the Miglyol® 812 (0.5 g) oil in a glass vial closed by a septum and stirred at 80°C in a water bath for 10 min to ensure homogeneity of the mixture. In parallel, water (8.5 g) was also heated to 80°C and progressively added to the organic mixture under constant stirring. The resulting dispersion was then removed from the bath and left to cool at room temperature.

1.3. Preparation of the organogel

The organogel was prepared by mixing the oil (Miglyol® 812) and the gelator (12-HOA, 1-25 % wt.) while stirring at 80°C to ensure complete solubilization. The resulting solution was then left to cool to room temperature.

2. Methods

2.1. Multi-speckle diffusing wave spectroscopy (MS-DWS)

MS-DWS measurements were performed using a Rheolaser CRYSTAL® (Formulaction, France), based on dynamic light scattering (DLS) of opaque media in backscattering mode using a 650-nm coherent laser. The light is multi-scattered by the particles, which leads to interfering backscattered waves. An interference image called a “Speckle image” is detected by a multi-pixel detector. The difference between two successive speckles are measured and computed using a correlation function. The result is used to determine the micro-dynamics of the sample, related to its viscoelastic behavior. All measurements were realized in the closed cell developed by Formulaction (France).

To determine the phase inversion temperature, a nanoemulsion containing 1% of polymer latex was analyzed. Two successive heating and cooling cycles were performed to check the reversibility of the

system. The temperature was first increased from 25 to 75 °C at a rate of 5°C/min to avoid phase separation at high temperatures, then decreased to 25°C at the same rate.

To determine the gelation kinetics of the gelled nanoemulsion, a closed cell pre-heated to 80°C was filled with the dispersion (also warmed to 80 °C) containing 1% of polymer latex as scattering agents, ensuring opacity. The filled cell was then placed in the device, which was set at 25°C. Microdynamics were monitored against time at 25°C.

2.2. Rheology

Rheological behaviors were measured using an advanced rheological expansion system (Advanced Rheometer AR-1000, TA Instruments). Oscillatory shear measurements were conducted in a stress-controlled rheometer system. The system used 40-mm stainless steel parallel plate geometry. The rheometer was equipped with a Peltier plate to control the temperature within 0.1°C of the set value. Nanoemulsions were put in place with a syringe. Gelled nanoemulsion samples were placed using a spatula to prevent the loss of mechanical properties. All experiments were performed in triplicate. The linearity domain was measured with oscillatory measurements at the frequency of 1 Hz and a temperature of 25°C. Linearity was determined by following the variations in the storage modulus (G') and the loss modulus (G'') with the oscillatory stress. G' and G'' were linear and stable between 0.2 and 5 Pa for both the nanoemulsion and the hydrogel.

For thermal behavior, measurements were started at 25°C and then increased until 70°C with a ramp rate at 1°C/min. Oscillation amplitude was controlled to obtain a stress of 1 Pa and the frequency was set at 1 Hz. Thermal behavior was determined by following the variations in the storage modulus (G') and the loss modulus (G'') with the temperature.

Frequency sweep measurements were conducted with the same material between 0.1 and 100 Hz at 25°C and a constant stress of 1 Pa.

2.3. Dynamic Light Scattering (DLS)

Particle hydrodynamic radii (Rh) and polydispersity indexes (PdI) were determined using dynamic light scattering (DLS). Routine experiments were first conducted at 25°C on a ZEN 3600 Zetasizer NanoZS (Malvern), operating in backscattering mode at 173° with a 4 mW He-Ne laser (wavelength: 633 nm). All measurements were performed at least five times. Mean size values were obtained as distribution profiles in intensity using the software from Malvern (cumulant analysis) and were averaged.

2.4. Multi-angle static- and dynamic light scattering (MASLS, MADLS)

In light scattering experiments, the scattering wave vector q is defined as described in equation (1):

$$q = \frac{4\pi n \sin(\theta/2)}{\lambda} \quad (1)$$

where θ is the scattering angle, n the refractive index of the solvent, and λ the wavelength of the incident light.

- **Multi-Angle DLS (MADLS)**

Multi-angle light scattering characterizations were performed on a 3D LS Spectrometer from LS Instruments (Fribourg, Switzerland) using a 100-mW high-performance DPPS Laser from Cobolt (λ = 660 nm), a two-channel multiple tau correlator (auto and cross correlation, 1088 real-time channels), a 3D cross-correlation module, a variable-angle detection system equipped with two high-sensitivity APD detectors. Cylindrical glass cells (10 mm diameter) containing the samples (1.1 mL) were placed in the sample chamber filled with index matching fluid (decaline), which was temperature-controlled using an external circulator (Julabo CF31). Measurements were performed at 25°C for scattering angles θ ranging from 12° to 150°, corresponding to scattering wave vectors q=[4π·n·sin(θ/2)]/λ ranging from 3×10-4 to 2×10-3 Å-1 (n=1.330 is the refractive index of water). Samples were opalescent and preliminary experiments indicated that they produced multiple scattering. Therefore, the 3D cross-correlation configuration25 was required to overcome this problem by discarding the multiple scattering contribution from the total scattered light. At each angle, 3 to 10 measurements were performed and averaged.

Performing dynamic light scattering experiments allow use of the autocorrelation function $g^{(2)}(q,\tau)$ of the scattered intensity $I(q,t)$, normalized over time (2):

$$g^{(2)}(q,\tau) = \frac{\langle I(q,t) I(q,t+\tau) \rangle}{\langle I(q,t) \rangle^2} \quad (2)$$

The correlation function for the electric field $g^{(1)}(q,\tau)$ is then obtained using the Siegert relationship (3):

$$g^{(2)}(q,\tau) = 1 + \beta \left| g^{(1)}(q,\tau) \right|^2 \qquad \beta \leq 1 \quad (3)$$

For monodisperse spherical particles under Brownian motion, the autocorrelation function decays exponentially over time (4):

$$g^{(1)}(q,\tau) = e^{-\Gamma\tau} \quad (4)$$

where $\Gamma = D_0 q^2$ is the decay rate and D_0 is the translational diffusion coefficient of the particles. The hydrodynamic radius (R_h) is then obtained using the Stokes-Einstein relationship (5):

$$R_h = \frac{kT}{6\pi\eta D_0} \quad (5)$$

where k is the Boltzmann constant, T the absolute temperature and η the solvent viscosity.

Experimentally, multiple scattering was always observed from the opalescent nanoemulsion and its dilutions. The 3D cross-correlation configuration was then required to remove this multiple scattering contribution. The autocorrelation functions obtained were then analyzed using the home-made MULTI-STORMS program developed by Dr. C. Mingotaud, written and compiled with MATLAB®. This software is designed for data analysis and offers the choice in the methods used to extract information from the correlograms and then to evaluate size distributions. Mathematical adjustments of the correlograms are performed using different algorithms based on the shape and the scattering properties of the particles to be analyzed. In the present case, the curves were well fitted with a 2nd order cumulant analysis based on the paper by Frisken,[1] and using equation (6):

$$g^2(\tau) = B + \beta \cdot e^{-2\bar{\Gamma}\tau} \cdot (1 + \frac{\mu_2}{2!}\tau^2 - \frac{\mu_3}{3!}\tau^3 + \ldots)^2 \quad (6)$$

where B is the background value, β the amplitude of the autocorrelation function, $\bar{\Gamma}$ the mean value of the decay rates and μ_n the nth moment of the distribution function of decay rates, $f(\Gamma)$. This analysis provided the intensity-weighted decay rates Γ. The plots of the decay rates as a function of q^2 gave linear slopes $\Gamma = D_{app}q^2$, indicating that single relaxation mechanisms were observed, associated with single apparent translational diffusion coefficients (D_{app}). Hydrodynamic radii were subsequently calculated from D_{app} using equation (5).

- **Multi-angle SLS (MASLS)**

In static light scattering, the excess of a sample's scattered intensity with respect to the solvent is converted into absolute intensity (Rayleigh ratio R_θ, in cm^{-1})[2] using toluene as a reference ($R_{\theta,toluene}$ = 1.19×10^{-5} cm^{-1} at 660 nm) as described in equation (7):

$$R_{\theta,sample} = \frac{I_{sample} - I_{solvent}}{I_{toluene}} \cdot \left(\frac{n_{solvent}}{n_{toluene}}\right)^2 \cdot R_{\theta,toluene} \quad (7)$$

where I_{sample}, $I_{solvent}$, and $I_{toluene}$ are the scattering intensities of the sample solution, the solvent and the toluene, respectively, and where $n_{solvent}$ and $n_{toluene}$ are the refractive indexes of the solvent and the toluene at 660 nm, respectively (n_{water} = 1.33 and $n_{toluene}$ = 1.49 at 25 °C).

Multi-angle static light scattering measurements were performed from 12° to 150° (q = 2.6×10^{-4}-2.4×10^{-3} $Å^{-1}$) on native nanoemulsion and on diluted samples.

2.5. Differential scanning calorimetry (DSC)

The T°gel and T°melt of the organogels were assessed using differential scanning calorimetry (Mettler Toledo, Viroflay, France) experiments. Organogels were prepared and 10-20 mg samples were placed in hermetically sealed aluminium pans. DSC runs were carried out with four heating-cooling cycles between 20 and 85°C at a constant rate of 3°C per minute, and with an empty aluminum pan used as reference. The first cycle was used to erase the thermal memory of the sample and was not analyzed. The sol-gel transition temperatures (Tgel) and gel-sol transition temperatures (Tmelt) were determined on thermograms with the STARe software provided by Mettler Toledo, and using peak temperatures.

3. Characterization of the nanoemulsion

After the preparation with the PIT process, the nanoemulsion appears translucent with blue glints, and possesses stability against creaming. The difference between the nanoemulsion obtained and the starter macroemulsion is shown Fig. S2.

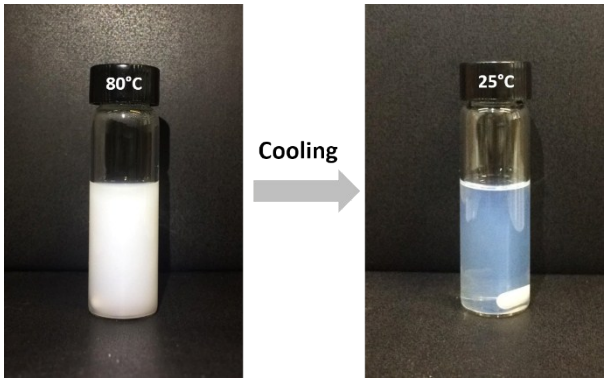

Fig. S2 Photographs of colloidal dispersions during the preparation steps illustrating the PIT process under cooling.

PIT can also be followed by optical observation using a microscope equipped with a heating plate. Micrographs during the cooling stage are shown in Fig. S3. The colloidal dispersion shows different aspects before and after the PIT, reflecting the change of scale of the droplets and the transition from an emulsion to a nanoemulsion. Dispersion begins to show a change of aspect at 73°C, corresponding to the bicontinuous phase between nanoemulsion and macroemulsion that is illustrated at 76°C. These observations confirm that the PIT starts at 72°C.

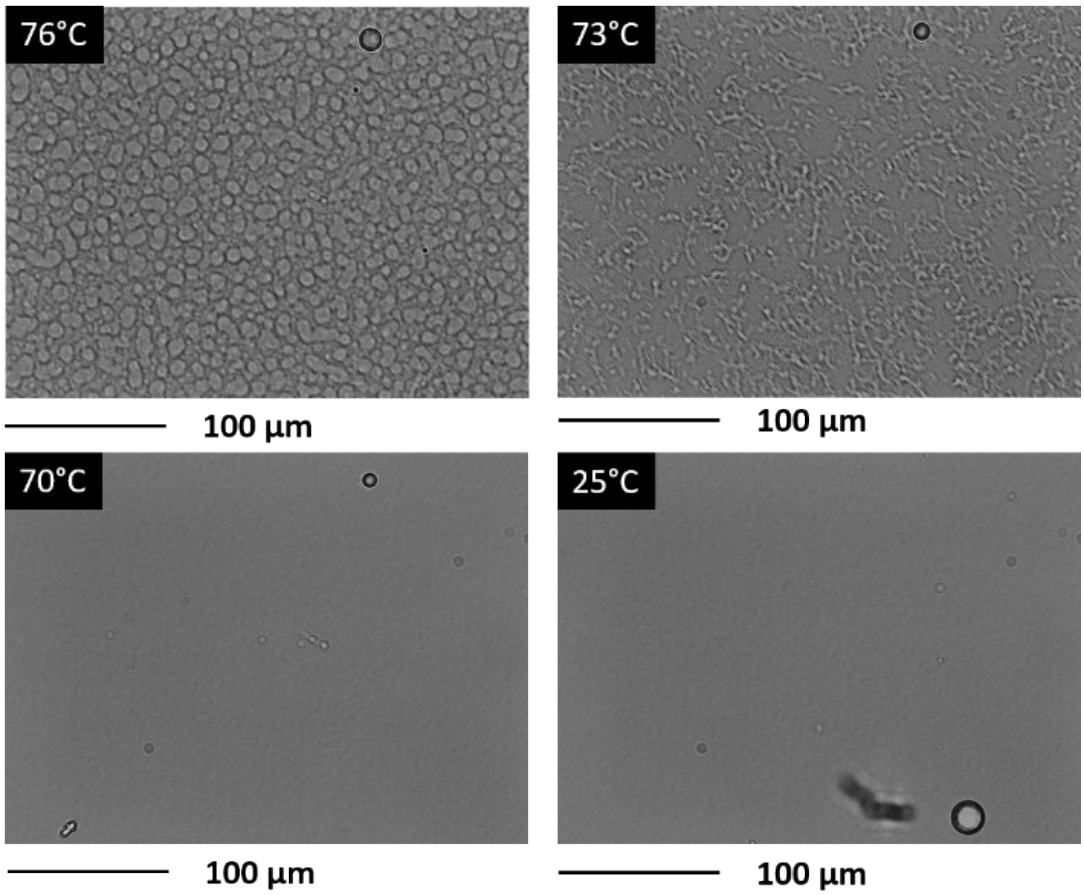

Fig. S3 Optical micrographs showing texture evolutions during nanoemulsion formation under cooling.

As illustrated in Fig. S4, PIT is characterized in MS-DWS by the increase of the micro-dynamic at 72°C due to the high mobility of the molecules during the phase inversion phenomenon.

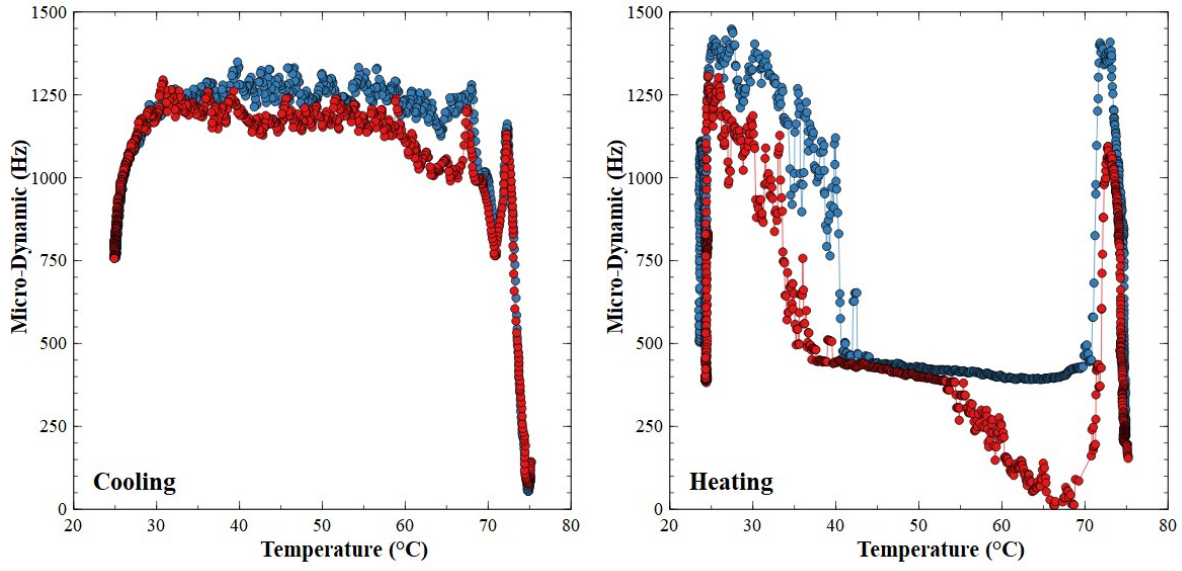

Fig. S4 MS-DWS measurements of the nanoemulsion, at the left under heating and at the right under cooling. For both heating and cooling, red dots represent the first cycle and blue dots represents the second cycle.

Rheological measurements are presented in Fig. S5 and show that the nanoemulsion storage modulus (G') is one order of magnitude higher than the loss modulus (G''). Increasing temperature above 54°C leads to a loss of both moduli. This loss appears to correspond to a loss of the interaction between particles that could be related to the high Brownian motion.

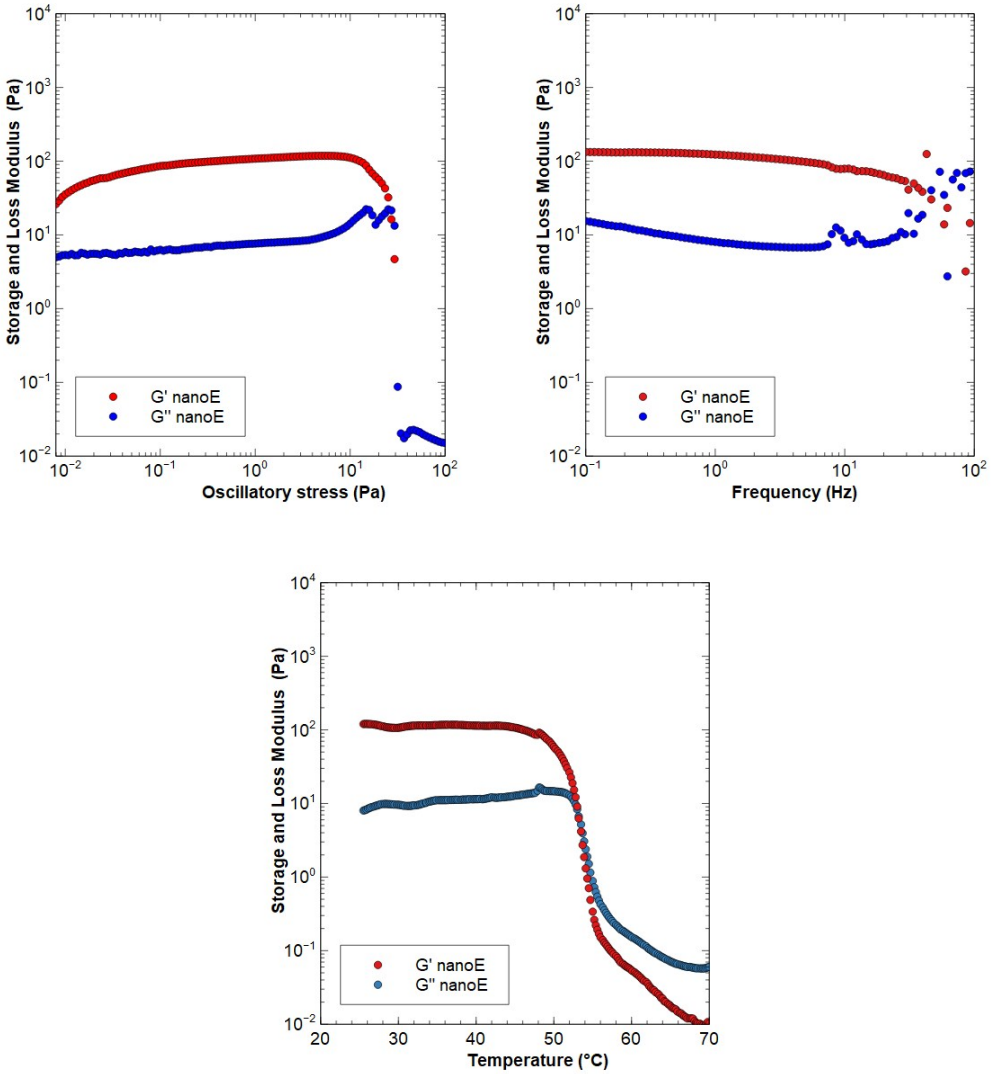

Fig. S5 Variations of the storage modulus (G') and the loss modulus (G'') of the nanoemulsion under different parameters. (top left) : Linearity domain; (top right) Frequency sweep measurements; (bottom) Thermal behaviour.

Sizes of the nanoemulsion droplets were followed by MADLS. The effect on aging on the nanoemulsion droplets is presented in Fig. S6 and shows an increase in size after few months.

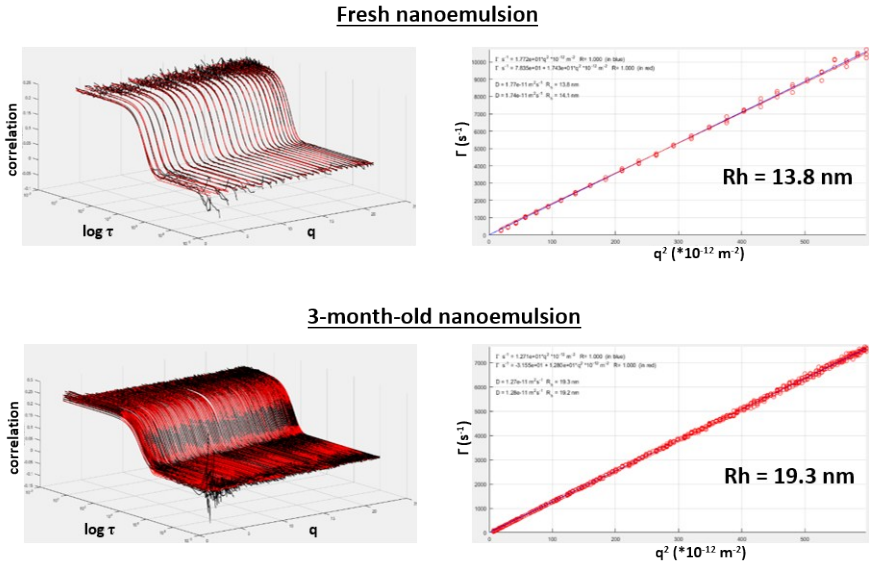

Fig. S6 Effects of aging on the size of nanoemulsion droplets. (right): correlograms recorded at various angles; (left): corresponding linear variations of decay rates Γ as a function of q^2.

Measurements were also performed on a series of diluted samples. Results are presented in Fig. S7 and show that multiple scattering was suppressed when dilution reached 1/10 and below. Moreover, the apparent hydrodynamic radii decreased from 13.8 nm to 8.6 nm upon dilution up to 1/20.

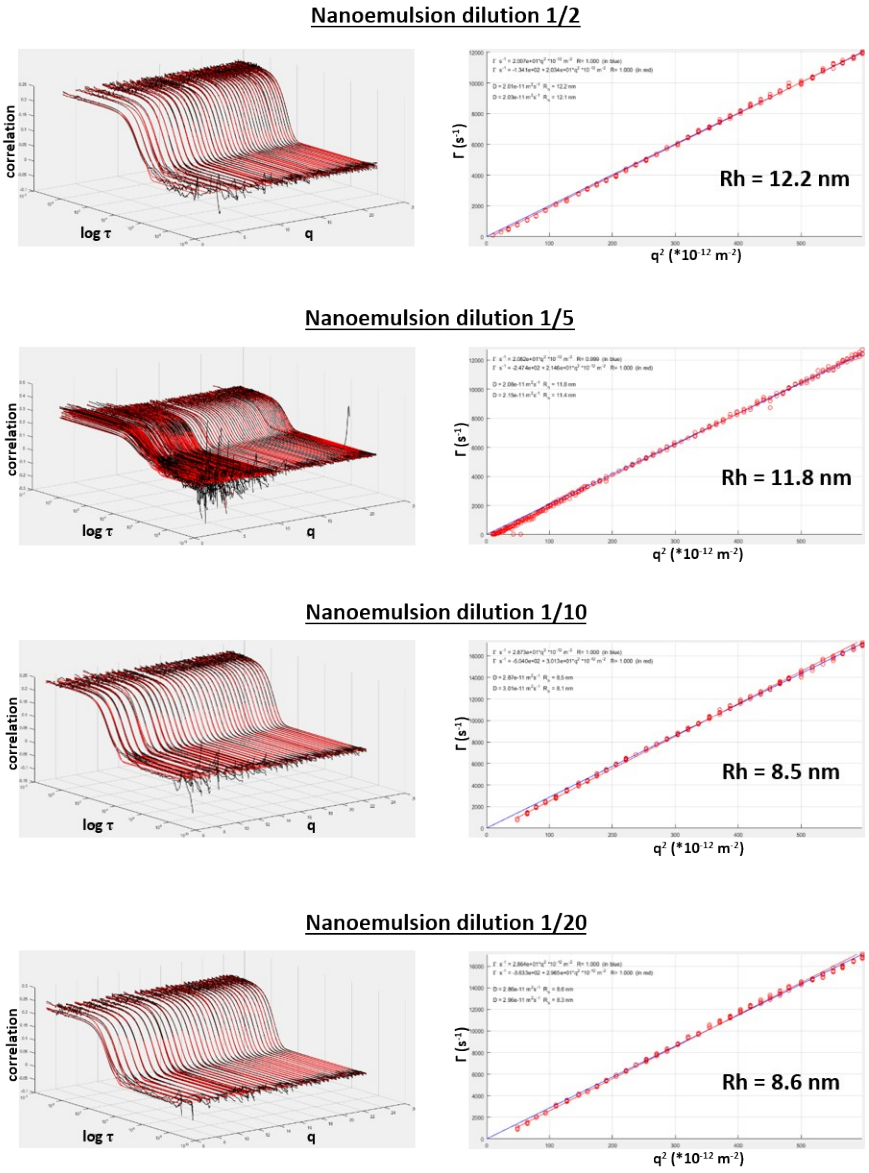

Fig. S7 Effects of dilution on the size of nanoemulsion droplets. (right): correlograms recorded at various angles; (left): corresponding linear variations of decay rates Γ as a function of q^2.

Absolute excess Rayleigh ratios as a function of q are reported in Fig. S8.

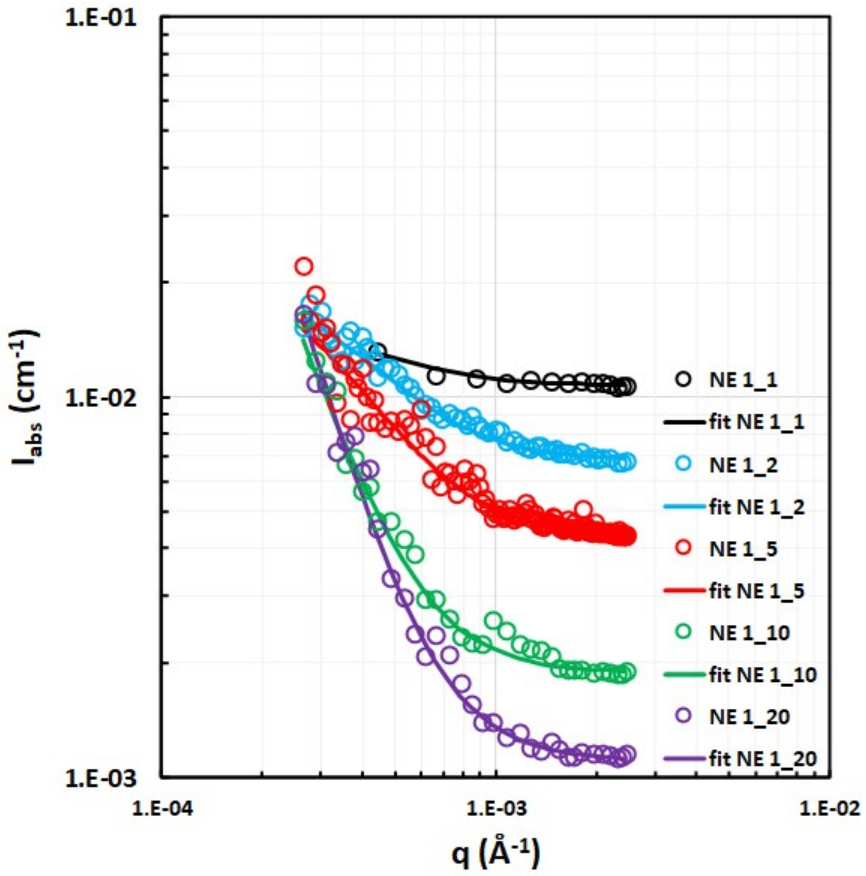

Fig. S8 MASLS profiles of the native nanoemulsion and its dilutions. Solid lines are the fits using a surface mass fractal model.

For each sample, the Rayleigh ratio was found to be constant from moderate to high q values (q > 1×10^{-3} Å^{-1}). This isotropic scattering indicated that the Guinier regime was not reached due to the very small particle sizes. Therefore, the radius of gyration R_g could not be determined in this q range (q-independent form factor). Scattering intensities increased at low q values, which could be related to the presence of a fractal network of particles due to attractive inter-particle interactions, as observed by others in the case of concentrated nanoemulsions.[3,4] The experimental scattering intensities were then fitted using a mass surface fractal model for the form factor P(q) described in equation (8), already implemented in the SasView fitting software:

$$P(q) = \left\{ \left[1 + (q^2 a)\right]^{\frac{D_m}{2}} \times \left[1 + (q^2 b)\right]^{\frac{6 - D_s - D_m}{2}} \right\}^{-1} \quad (8)$$

$$a = R_g^2 / (\frac{3D_m}{2})$$

$$b = \frac{r_g^2}{\left[-\frac{3(D_s + D_m - 6)}{2}\right]}$$

where R_g and r_g are the sizes of the cluster and the primary particle, respectively, and where D_s and D_m are the surface and mass fractal dimensions, respectively.

Complementary SAXS experiments were also carried out to get more information on the nanoemulsion droplets. The general expression of the scattered intensity $I(q)$ is given by equation (9):

$$I(q) = \Phi \cdot V \cdot (\Delta\rho)^2 \cdot P(q) \cdot S(q) \quad (9)$$

where $q = [4\pi \sin(\theta/2)]/\lambda$ is the scattering vector (θ is the scattering angle), Φ is the volume fraction of the scatterers, V is their volume and $\Delta\rho$ is their difference in scattering length density (SLD) with respect to the solvent. $P(q)$ is the scatterers' form factor and $S(q)$ is the structure factor accounting for inter-particle interactions, for which various analytical models are available.[5,6]

Experimental SAXS profiles obtained for the nanoemulsion and its dilutions are reported in Fig. S9.

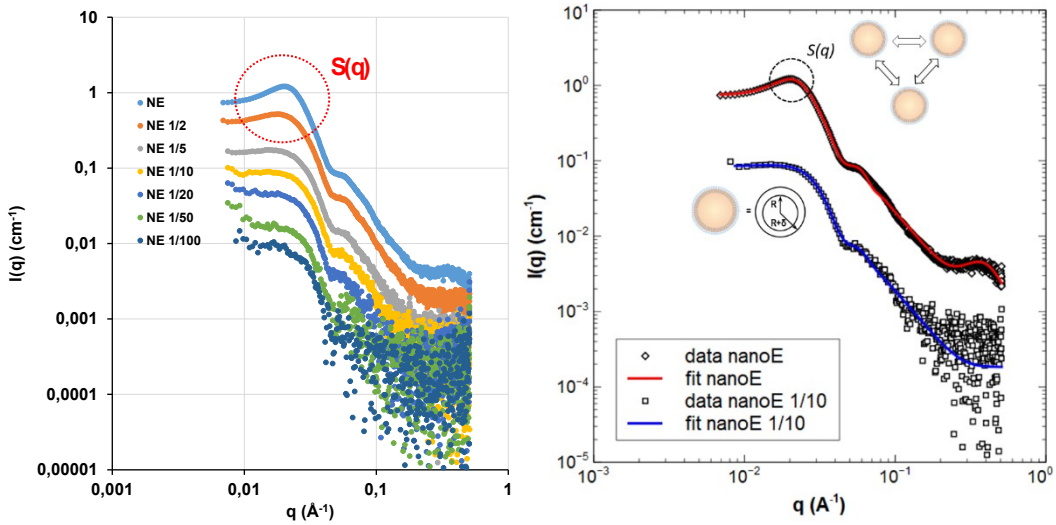

Fig. S9 SAXS profiles representing the scattered intensity I(q) in absolute units as a function of q as recorded for the nanoemulsion and its successive dilutions. (left) SAXS profiles obtained for the nanoemulsion (open diamonds) and the 1/10 diluted nanoemulsion (open squares). Solid lines are fits using a core-shell model as the form factor combined with a sticky hard sphere structure factor in the case of the concentrated sample. (right)

For concentrated samples, inter-particle interactions are responsible for the appearance of a broad peak related to the structure factor. The form factor P(q) was determined on the 1/10 dilution where

S(q)=1, using the SasView software. In this case, the SAXS profile could be suitably adjusted using a core-shell form factor as described in equation (10):

$$P(q) = \frac{\emptyset}{V_s} F^2(q) \quad (10)$$

with

$$F(q) = \frac{3}{V_s}\left[V_c(\rho_c - \rho_s)\frac{\sin(qr_c) - qr_c\cos(qr_c)}{(qr_c)^3} + V_s(\rho_s - \rho_{solv})\frac{\sin(qr_s) - qr_s\cos(qr_s)}{(qr_s)^3}\right]$$

where V_s and V_c are the volumes of the shell and the core, respectively; r_c is the radius of the core and r_s = r_c + thickness (δ) is the radius of the particle; ρ_c, ρ_s, and ρ_{solv} are the scattering length densities of the core, the shell and the solvent, respectively.

For concentrated samples, this P(q) core-shell model was combined with a sticky hard sphere model S(q) to successfully fit the SAXS profiles. This model takes into account attractive inter-particle interactions by using a narrow attractive well. The full description of S(q) can be found in the literature.[7,8]

Complementary cryo-SEM observations show that droplets are rather homogeneous with a spherical aspect as illustrated in Fig. S10. The apparent mean diameter of the droplets is about 20-30 nm.

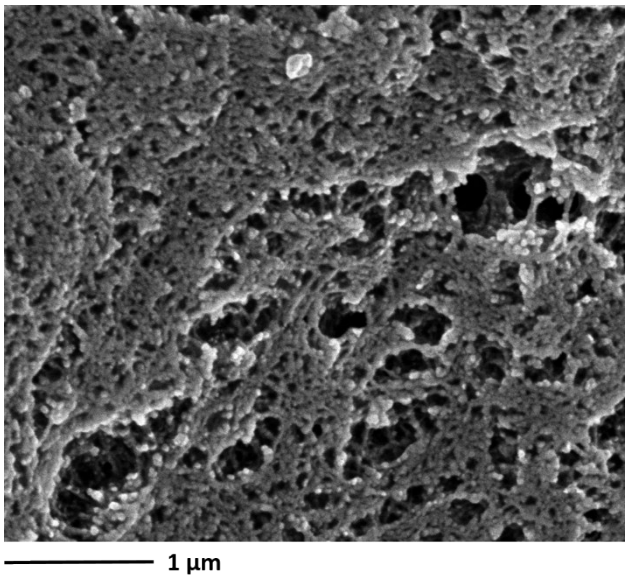

Fig. S10 Cryo SEM micrograph of nanoemulsion.

4. Characterization of the organogel

The formation of the organogel under cooling is illustrated by the inverted bottle test in Fig. S11.

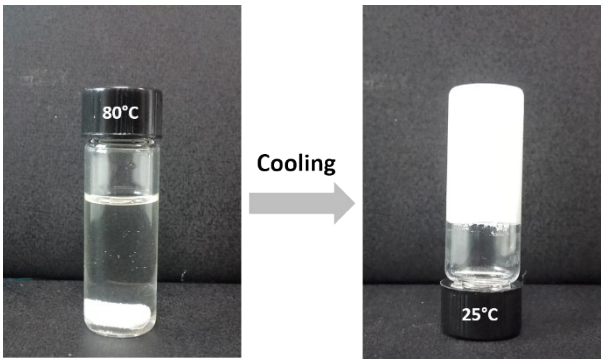

Fig. S11 Photographs of organogel (20 % wt. of 12-HOA) before and after gelation.

The phase diagram for Miglyol® 812 / 12-HOA was determined by plotting T°gel/T°melt against the concentration of 12-HOA. For all the samples T°gel was below 60°C and T°melt below 70°C.

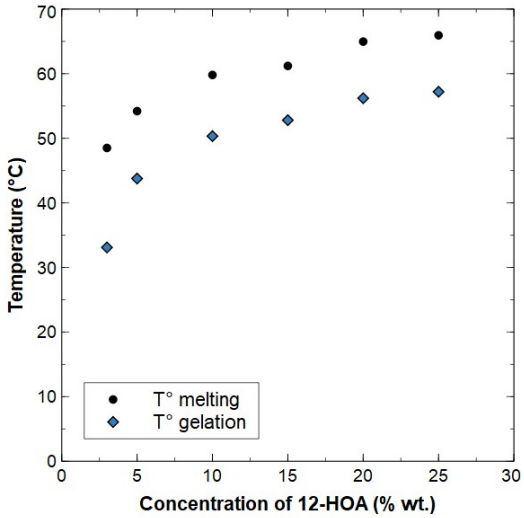

Fig. S12 Sol-Gel phase diagram for 12-HOA in Miglyol 812 obtained by DSC.

Micrographs of 20 % wt. 12-HOA in Miglyol® 812 under cooling are reported in Fig. S13 and show the gelation at 61°C.

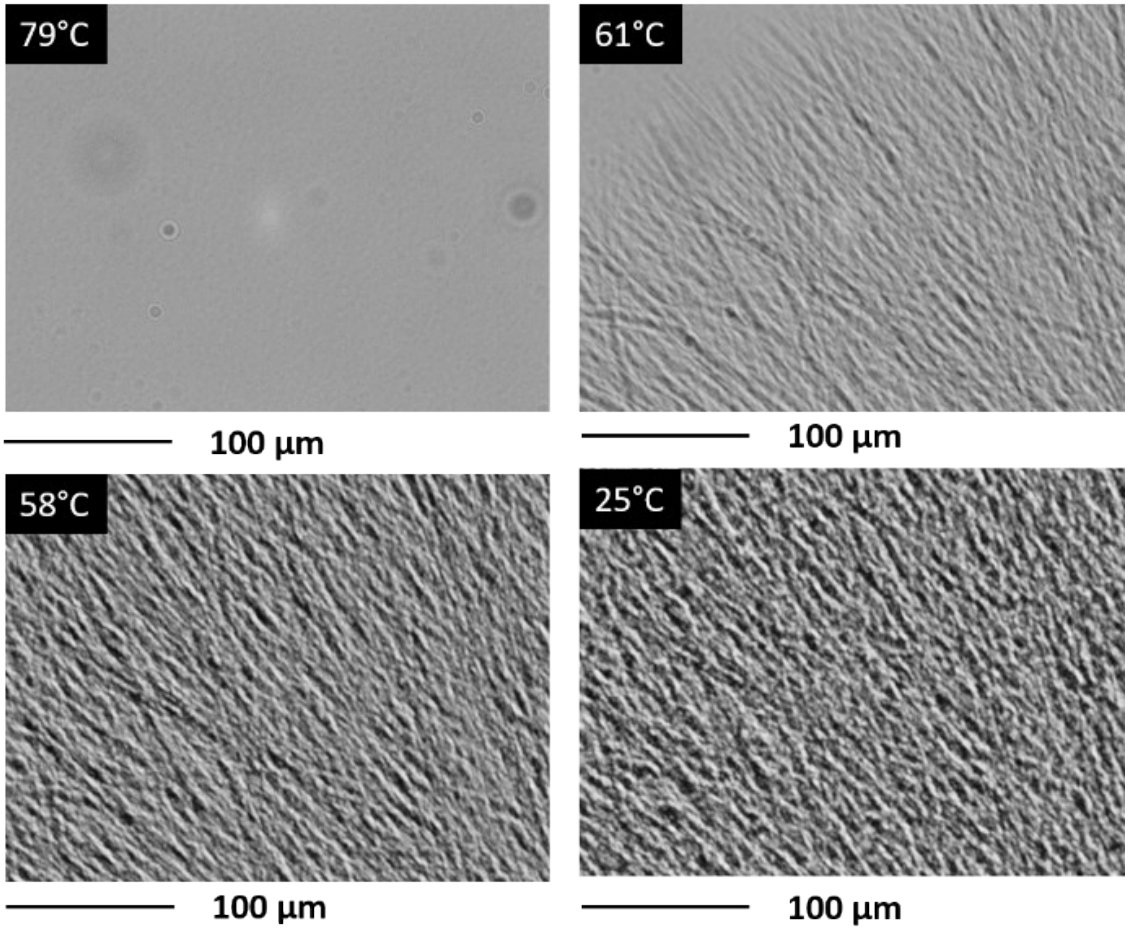

Fig. S13 Optical micrographs of organogel during the cooling stage.

The model used to adjust the organogel SAXS profile was based on the consideration that the scattered intensity originated from the contributions of both the infinitely long cylinders (organogel fibers) and the lamellae (junction nodes)[9]:

$$I(q) = I_{cylinders} + I_{lamellae} \tag{11}$$

with

$$I_{cylinders}(q) = \emptyset \cdot \frac{r^2 \Delta\rho^2}{2q} \cdot \left[\frac{J_1(qr)}{qr}\right]^2 \tag{12}$$

where Ø is the volume fraction, *Δρ* the scattering length density difference, *r* the radius of the cylinder and J_1 the first order Bessel function,

and with

$$I_{lamellae}(q) = \emptyset \cdot \frac{2\pi}{q^2 T} \cdot \frac{4\Delta\rho^2}{q^2} \cdot \sin^2\left(\frac{qT}{2}\right) \tag{13}$$

where Ø is the volume fraction, *Δρ* the scattering length density difference and *T* the layer thickness.

An additional contribution was also added as a Gaussian function to take into account the presence of a Bragg peak:

$$I_{Gauss}(q) = scale \cdot exp\left(-\frac{(q-q_0)^2}{2\sigma^2}\right) + I_b \quad (14)$$

where *scale* is the height of the peak centered at q_0 with a standard deviation σ and I_b is the background intensity.

Experimental data and associated fit are presented in Fig. S14.

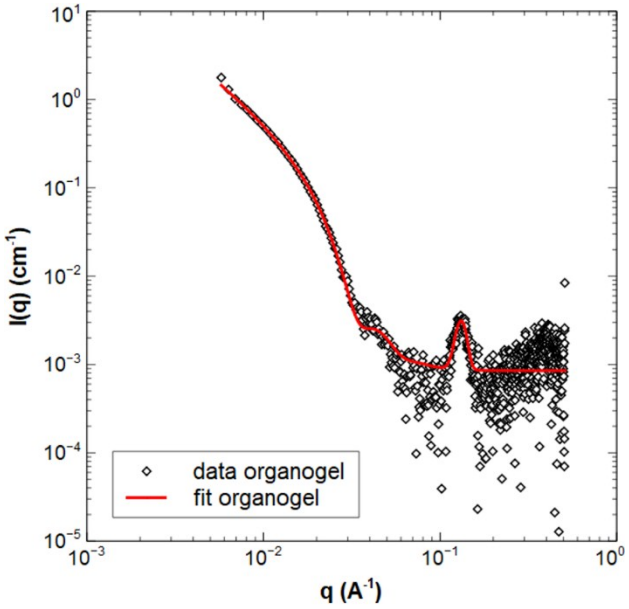

Fig. S14 SAXS profile (open diamonds) of a 1% wt. HOA gel in Miglyol® 812. The solid red line is the fit of the data using a model of an interconnected fibrillary network including a Bragg peak.

5. Complementary characterization of the gelled nanoemulsion

Gelation kinetics of the gelled nanoemulsion can be determined by multi-speckle diffusing wave spectroscopy (MS-DWS) by following micro-dynamic over time. Results are presented in Fig. S15 and show that gel is stable after 3 days.

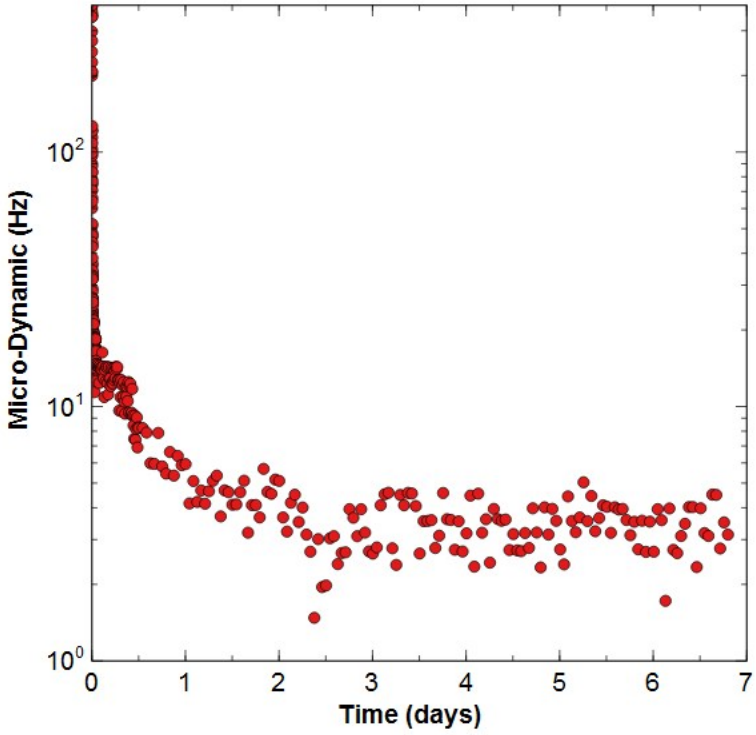

Fig. S15 Gelation Kinetics of hydrogel at 25°C as observed by MS-DWS.

Rheological measurements of the gelled nanoemulsion are presented in Fig. S5 and confirm the formation of a gel with a storage modulus (G') higher than the loss modulus (G''). Upon heating G' and G" decrease and cross at 43°C indicating melting of the gel.

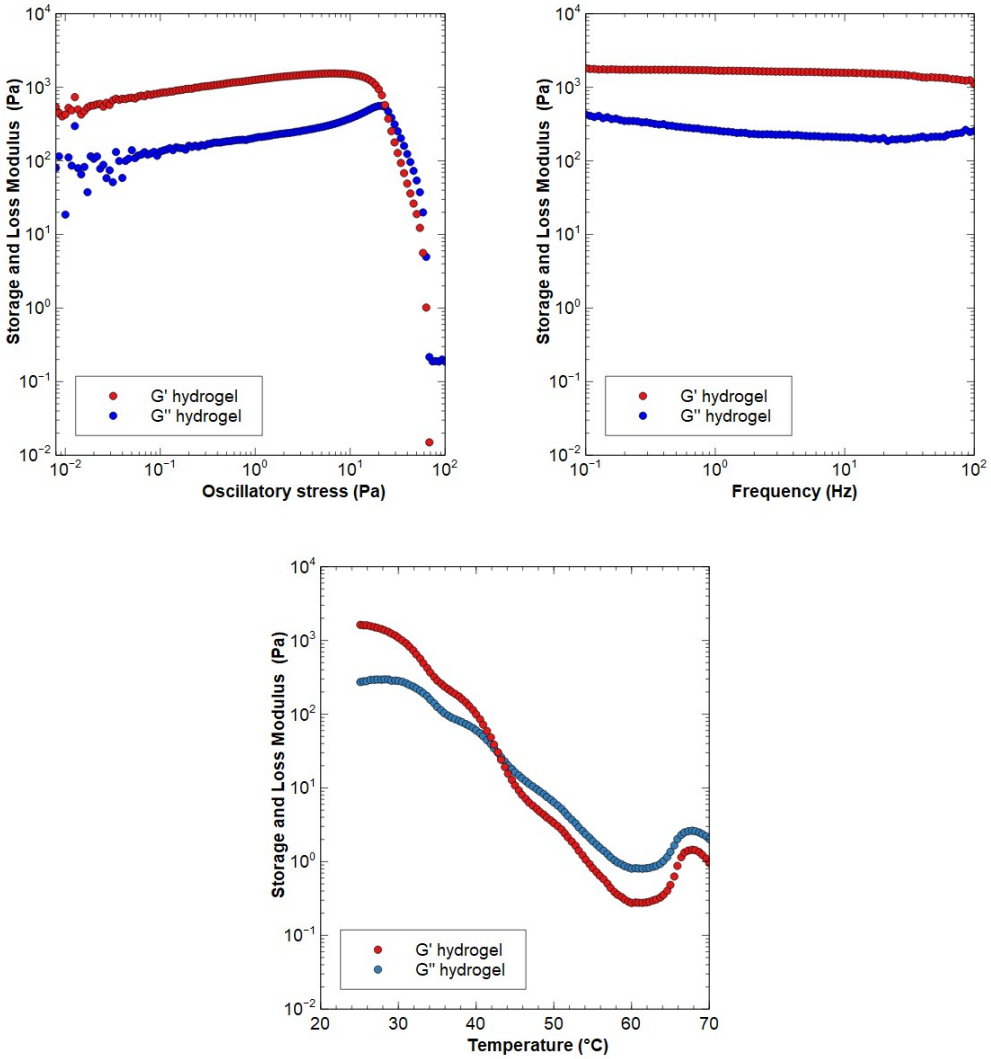

Fig. S16 Variations of the storage modulus (G') and the loss modulus (G'') of the gelled nanoemulsion under different parameters. (top left) : Linearity domain; (top right) Frequency sweep measurements; (bottom) Thermal behaviour.

6. References

1 B. J. Frisken, *Appl. Opt.*, 2001, **40**, 4087–4091.

2 H. Wu, *Chem. Phys.*, 2010, **367**, 44–47.

3 J. N. Wilking, S. M. Graves, C. B. Chang, K. Meleson, M. Y. Lin, and T. G. Mason, *Phys. Rev. Lett.*, 2006, **96**, 015501.

4 M. E. Helgeson, Y. Gao, S. E. Moran, J. Lee, M. Godfrin, A. Tripathi, A. Bose, and P. S. Doyle, *Soft Matter*, 2014, **10**, 3122–3133.

5 J. S. Pedersen, *Adv. Colloid Interface Sci.*, 1997, **70**, 171–210.

6 J. S. Pedersen, in *Neutrons, X-rays and Light: Scattering Methods Applied to Soft Condensed Matter*, 2002. Th. Zemb and P. Lindner ed. (North Holland)

7 S. V. G. Menon, C. Manohar, and K. Srinivasa Rao, *J. Chem. Phys.*, 1991, **95**, 9186–9190.

8 D. Gazzillo and A. Giacometti, *J. Chem. Phys.*, 2004, **120**, 4742–4754.

9 M. Laupheimer, T. Sottmann, R. Schweins, and C. Stubenrauch, *Soft Matter*, 2014, **10**, 8744–8757.